ELSEVIER

PII: S0032-3861(97)00159-6

Polymer Vol. 38 No. 24, pp. 5991–5999, 1997

0032-3861/97/$17.00 + 0.00

Application of an elastic model to the large deformation, high temperature stretching of polypropylene

J. Sweeney, T. L. D. Collins and P. D. Coates
Department of Mechanical and Manufacturing Engineering/IRC in Polymer Science and Technology, University of Bradford, Bradford BD7 1DP, UK

and I. M. Ward*
IRC in Polymer Science and Technology, University of Leeds, Leeds LS2 9JT, UK
(Revised 5 February 1997)

A physically based constitutive law for the deformation of polymers is applied to the stretching of polypropylene to large deformations at elevated temperatures. In this deformation regime, which is applicable to many forming processes, necking of the material is a persistent feature. The theory is elastic in nature, but includes the necking phenomenon as an inherent property. It is incorporated into a commercial finite element code and used to model a number of different experimental modes of deformation, both uniaxial and biaxial. Comparison is made with the experiments and it is found that both strains and forces are represented realistically, even though the true nature of the material is viscoelastic. Some of the discrepancies in the model predictions are traceable to its elastic nature. © 1997 Elsevier Science Ltd.

(Keywords: multiaxial drawing; polymer network; finite elements)

INTRODUCTION

In a variety of industrial forming processes, polymers are deformed in the solid phase to large strains at elevated temperatures. In some cases the process involves a stage of inhomogeneous deformation ('necking'). With this in mind, we demonstrated in a previous publication[1] an elastic constitutive law, for which the development of necking is an inherent feature.

In this paper we discuss the quantitative application of this material model to the stretching of polypropylene in various modes at 150°C. The procedures required to fix the values of the various parameters are demonstrated. These include the particular experimental techniques necessary to extract stress–strain information from inhomogeneously deforming specimens. Finite element modelling is used to analyse the complex deformation fields and associated drawing forces generated when specimens are stretched in both uniaxial and biaxial modes. By this means we evaluate the effectiveness of the theory. Because we know from a wide range of other experimental evidence that polypropylene is a viscoelastic material, there must be limitations to the general effectiveness of the analysis used. However, an elastic analysis has advantages from the point of view of computing. The realistic features of the model in its present form suggest that it could form the basis of a more comprehensive viscoelastic model.

The polymer is below its melting point at the temperature of testing and from a structural viewpoint consists of crystalline and amorphous regions. At a molecular level it is, therefore, not homogeneous. In spite of this it will be shown that the constitutive law used, which represents a single continuum, does provide a first-order description of the deformation behaviour. It is recognized that a more sophisticated model, taking into account differences in behaviour between crystalline and amorphous material, is likely to be more appropriate and provide a better quantitative description, and present efforts are directed towards this objective. However, in view of its simplicity of implementation in currently available finite element software, we have proceeded with the assumption of a homogeneous structure and will show that this provides an adequate description of the main features of the deformation behaviour.

THEORY AND IMPLEMENTATION

The development of the theory was given fully previously[1], and will only be summarized here. It is based on the model of Ball *et al.*[2]. This is a hyperelastic model in which the change in strain energy density W as a result of a deformation, defined by principal extension ratios λ_1, λ_2 and λ_3, is

$$\frac{W}{kT} = \frac{1}{2}N_c\sum_{i=1}^{3}\lambda_i^2 + \frac{1}{2}N_s\sum_{i=1}^{3}\left(\frac{(1+\eta)\lambda_i^2}{1+\eta\lambda_i^2} + \ln(1+\eta\lambda_i^2)\right) \quad (1)$$

where W is the energy per unit volume, k is Boltzmann's constant, T is the absolute temperature, N_c and N_s are, respectively, the number per unit volume of crosslinks

* To whom correspondence should be addressed

and sliplinks, and η is a parameter defining the extent of the motion of the sliplinks. η is non-negative, with the value zero corresponding to a state of fixed sliplinks, for which the theory reduces to the Gaussian chain model. For convenience we rewrite equation (1) as

$$W = \frac{1}{2}N_c^* \sum_{i=1}^{3} \lambda_i^2 + N_s^* \sum_{i=1}^{3} b(\lambda_i) \quad (2)$$

where $N_c^* = kTN_c$ and $N_s^* = kTN_s$.The incompressibility condition $\lambda_1\lambda_2\lambda_3 = 1$ is assumed to apply. Given this constraint, equation (1) can be rewritten in terms of the invariants:

$$I_1 = \lambda_1^2 + \lambda_2^2 + \lambda_3^2, \quad I_2 = \lambda_1^2\lambda_2^2 + \lambda_2^2\lambda_3^2 + \lambda_3^2\lambda_1^2$$

as

$$W = \frac{1}{2}N_c^* I_1 + \frac{1}{2}N_s^* \left[\frac{(1+\eta)(I_1 + 2\eta I_2 + 3\eta^2)}{1 + \eta I_1 + \eta^2 I_2 + \eta^3} + \ln(1 + \eta I_1 + \eta^2 I_2 + \eta^3) \right] \quad (3)$$

The constitutive equations for the stresses $\sigma_{ii}(i = 1, 2, 3)$ are given by

$$\sigma_{ii} = \lambda_i \frac{\partial W}{\partial \lambda_i} - p \quad (4)$$

where the incompressibility assumption has led to the appearance of a hydrostatic pressure p. Substituting equation (2) into equation (4) gives

$$\sigma_{ii} = N_c^* \lambda_i^2 + N_s^* \lambda_i b'(\lambda_i) - p \quad (5)$$

Following some initial studies on the application of this model to stretching of polymer sheets[3], a modification was introduced[1] in the form of the addition of strain dependence in N_s^* to this constitutive equation. A decrease in N_s^* with increasing strain had the effect of allowing the onset of necking, corresponding to a minimum in the nominal stress–stretch curve, to occur at lower strains, in closer agreement to experimental observation. N_s^* was assumed to depend on the first invariant only, so the theory took the form:

$$\sigma_{ii} = N_c^* \lambda_i^2 + N_s^*(I_1)\lambda_i b'(\lambda_i) - p \quad (6)$$

N_s^* was assumed to vary between an initial value N_{s0}^* and an ultimate value $N_{s\infty}^*$, according to the relation:

$$N_s^*(I_1) = \frac{N_{s0}^* - N_{s\infty}^*}{(I_1 - 2)^\beta} + N_{s\infty}^* \quad (7)$$

where the exponent β controls the rate of decay of N_s^*.

Once the variation in N_s^* has been introduced, the theory embodied in equations (6) and (7) remains elastic in the Cauchy sense (stress depends only on the current strain), but is no longer hyperelastic, since the strain energy depends on the deformation path and a strain energy function does not exist. This is discussed fully in ref. 1. In spite of this the model has been implemented using the 'hyperelastic' facility in the finite element package ABAQUS. This is possible because the ABAQUS solution uses a constitutive equation depending on the derivatives $\partial W/\partial I_1$ and $\partial W/\partial I_2$. The required quantities were obtained by differentiating equation (3) (assuming N_s^* to be constant) and then replacing the constant N_s^* with the function of equation (7). These and other higher order derivatives required for the solution were generated as blocks of Fortran using a symbolic algebra package.

The finite element models used are of three experimental specimens to be discussed below. The meshes are illustrated in *Figures 6*, *13* and *16*. Four-noded bilinear quadrilateral elements are used throughout. For the models of sheet specimens of *Figures 13* and *16*, plane stress elements are used, while for the axisymmetric model of *Figure 6* hybrid elements were required to accommodate the assumption of incompressibility in the constitutive relation. The models of *Figures 6* and *13* are of uniaxial specimens, and the highest density of elements is in the gauge length where the necks form. The effect of changing the number of elements in this region was explored to establish convergence, and the present models were accepted on the basis that halving the number of these elements, by doubling their heights, resulted in essentially the same deformation fields and boundary forces. A similar approach, of studying the effect of changes in the element density in high strain regions, was adopted for the model of *Figure 16*. Here, in the high strain regions as discernible from the deformed model, the number of elements per unit length in the stretching (horizontal) direction was varied and convergence of the present model was established.

EXPERIMENTAL

The polypropylene copolymer material was manufactured by Tiszai Vegyi Kombinat, Hungary, and designated as grade K-899 and is the same as that used previously[1]. It was obtained both as granules and in commercial sheet form. Molecular weights as obtained by gel permeation chromatography were weight average $\bar{M}_w = 452\,600$ and number average $\bar{M}_n = 95\,760$. All the tests were carried out in air-blown ovens at 150°C.

For one class of experiment, specimens of cylindrical cross section were stretched uniaxially while being held in split collet grips. The dumb-bell geometries were machined from a solid billet of material. The billet was formed from the granules by filling a mould with melt from a single-screw extruder at an exit temperature of 230°C. The cylindrical mould was filled from below, with a weight resting on top of the extrudate, and then transferred to an oven at 180°C where it was stored for 6 h before being slowly cooled. Specimen geometries are illustrated in *Figure 1a*.

A second class of experiment also involved uniaxial stretching, but on plane specimens cut from the sheets. The geometry is illustrated in *Figure 1b*. Both these and the cylindrical specimens described above were stretched using an Instron testing machine at constant speeds corresponding to initial octahedral shear strain rates of 0.005, 0.01 and 0.02 s^{-1}, respectively.

All the uniaxial tests produced necking of the specimens, and so the measurement of strain was a non-trivial problem. Lines were marked on the specimen surfaces and they were observed through the glass oven door throughout the test. Strains at the surface were deduced from digitized images using the image analysis technique described previously[4]. For each test, 16 images were captured, equally spaced in time.

The material at this temperature is viscoelastic, and yet we are to make use of an elastic constitutive law. This means that we are to neglect the rate dependence of the

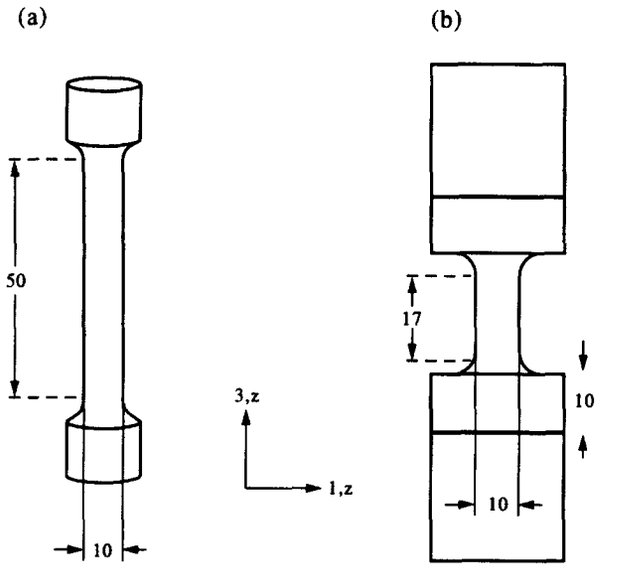

Figure 1 Geometries of uniaxial specimens: (a) cylindrical and (b) plane (1.6 mm thickness), where the thick horizontal lines define the extent of the gripping area. Dimensions in mm

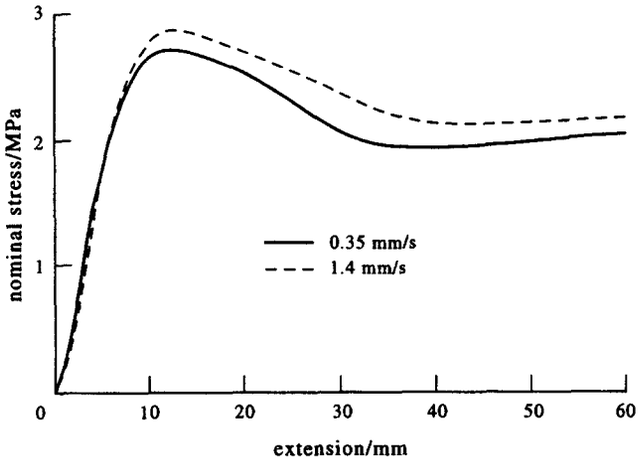

Figure 2 Experimental nominal stress–extension curves, for cylindrical specimens, showing the effect of testing rate

material. To give an initial assessment of the significance of this, we compare the load–extension curves for experiments at different rates. Once the specimen has begun to neck, the strain rate is not constant throughout and is not simply related to the testing speed. However, for extension ratios less than that corresponding to the force maximum, the specimens are homogeneous and the strain rates are proportional to the testing speeds. The comparison is made in *Figure 2* for speeds differing by a factor of four. The heights of the peaks in nominal stress differ by 5%, which is consistent with the rate dependence of this material when stretched in the form of thin sheets at 150°C[1]. The results suggest that data from experiments can be used successfully to model other processes without taking account strain rate, provided that the experiments and processes are conducted at comparable speeds.

More complex stretching experiments were performed in which forces were applied to sheet specimens along two perpendicular axes. The boundary conditions were such as to correspond with planar extension or stretching at constant width, with the added complication of

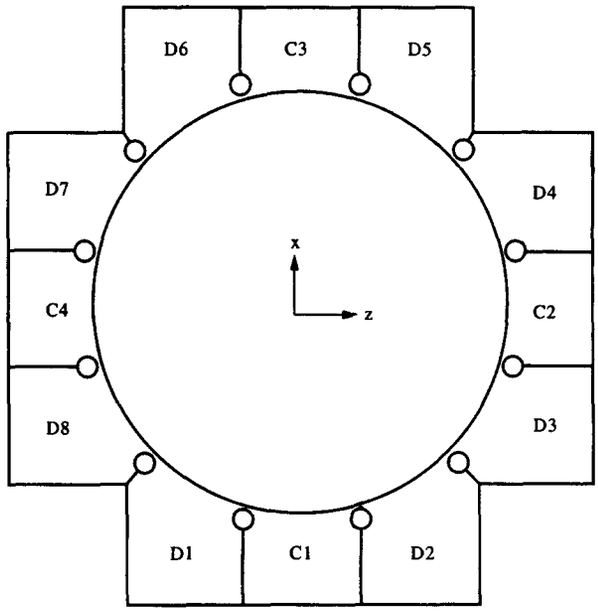

Figure 3 Specimen for planar extension experiments. Inner circular region is machined to approximately half the thickness of the original (1.6 mm thick) sheet. Gripped areas D6, C3 and D5 and D1, C1 and D2 separate as the specimen is extended in the z direction

inhomogeneous deformation. The specimen geometry is illustrated in *Figure 3*. There is a circular area which has been reduced in thickness to approximately half that of the original sheet; this is to ensure that deformation takes place within the interior of the specimen. Without this feature, specimens neck and extend around the grip area, leaving the specimen interior largely undeformed. The specimen is stretched in a biaxial testing machine manufactured in-house (the same one as in ref. 3) by being gripped at the tabs C1–C4 and D1–D8, which are separated by slits. Stretching is in the z direction, with lateral deformation in the x direction being restrained. Applied forces in both z and x directions are recorded. On extension, necking takes place, with necks initiating at the ends of the slits between separating tabs (i.e. between D7 and D6, D6 and C3, etc.). Photographs of undeformed and deformed specimens are shown in *Figure 4*. As with the uniaxial tests, the specimens were held in an air-blown oven at a temperature of 150°C, Initial shear strain rates were $0.01\,s^{-1}$. Deformations were measured by means of a mesh printed on the specimen surface, with direct measurements of it being made on the deformed specimen after testing.

RESULTS AND DISCUSSION

Derivation of parameter values

We require values of the parameters N_c^*, N_{s0}^*, $N_{s\infty}^*$, η and β. To obtain these we use information derived experimentally on both the deformed shapes of the specimens and the drawing forces. Traditionally, the uniaxial stress–strain curve is the source of data for fixing mechanical parameters. However, for a theory of this level of complexity, this special deformation provides insufficient information, and in particular fails to yield a unique value for η. There is the added problem that, while the uniaxial experiment can provide some of the information we require, truly uniaxial data are difficult to obtain from a necking specimen as a result of

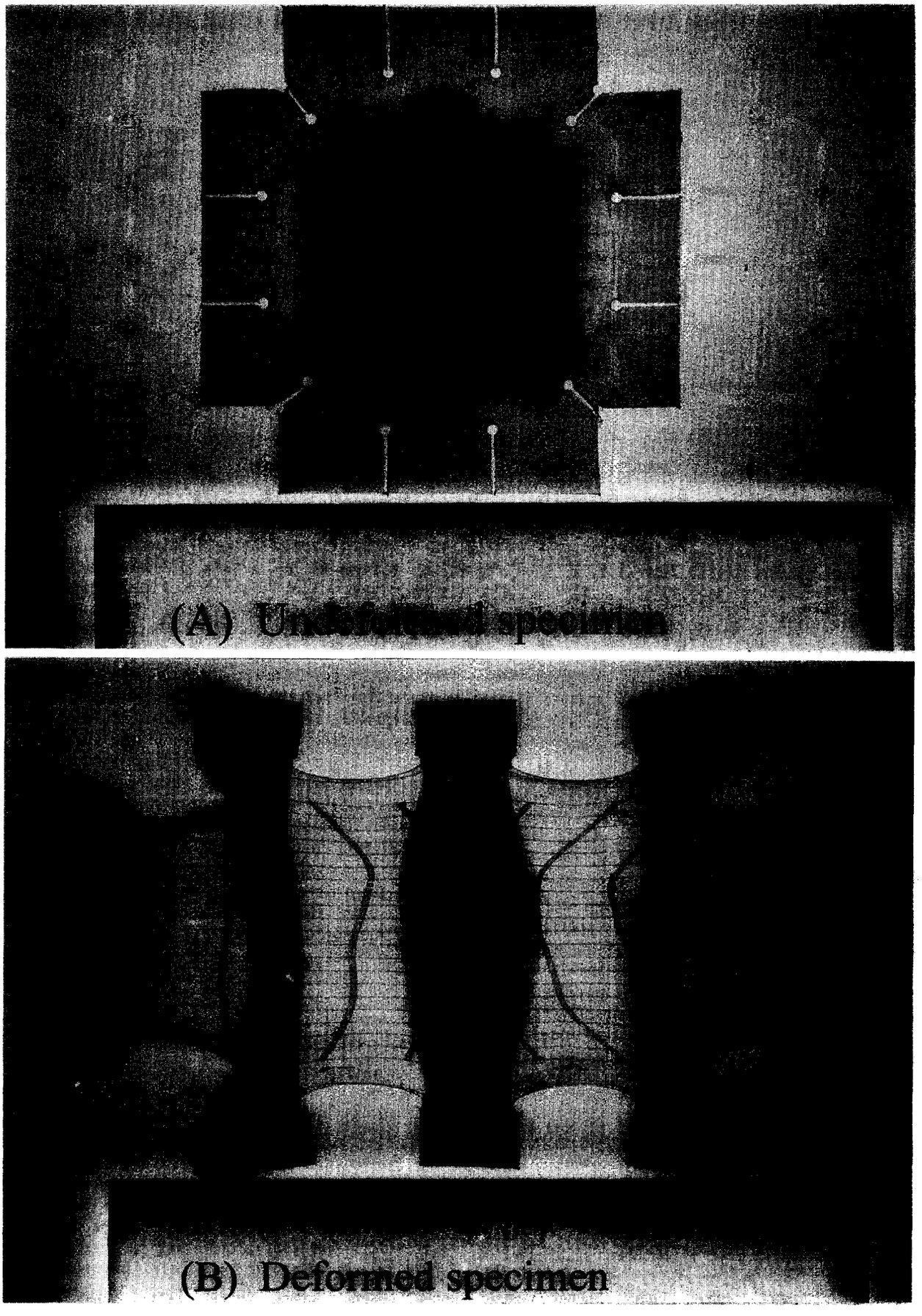

Figure 4 Photographs of planar extension specimens in (A) undeformed and (B) deformed states

the presence of shear stresses in the neck. An iterative process is therefore used, in which parameter values are estimated and then both applied forces and the shapes predicted by finite element models are compared with experiment. The forces, both axial and lateral, which are observed in the planar extension experiments are particularly crucial in fixing the value of η.

Uniaxial data

For incompressible material, the nominal stress is given by

$$\sigma_{33}^{n} = \sigma_{33}/\lambda_3 \tag{8}$$

where it is assumed that stretching is uniaxial along the 3 direction. Such a deformation is defined by principal extension ratios $(\lambda_3^{-1/2}, \lambda_3^{-1/2}, \lambda_3)$. *Figure 5* shows a curve of nominal stress against extension ratio for uniaxial stretching. This curve is typical of that of a necking polymer, with principal features the initial maximum, corresponding to the onset of necking, and the minimum at the higher extension which corresponds to the natural draw ratio. A realistic set of parameters must model the positions of these two features adequately. The basic phenomenology linking the stress–strain and the necking behaviour is well known[5]. The cylindrical tensile specimens come closest to pure uniaxial deformation, since the symmetry ensures that $\lambda_1 = \lambda_2$. However, only in regions of the specimen where there is no shear, such as at the centre of the neck, is the deformation truly uniaxial. The strains measured by image analysis cannot therefore be simply interpreted to define a uniaxial stress–strain curve. If we are able to observe the centre of the neck, then the strains there do indeed allow this simple interpretation, but in general the surface strains provide information which should be interpreted less directly, such as by comparison with those predicted by a finite element analysis.

Such a model is shown in *Figure 6*. The axisymmetric model of half the specimen is made with four-noded elements using the package ABAQUS. The values of the modified Ball *et al.* model parameters are the set designated A in *Table 1*. These were arrived at by a process of trial and error. The ratios N_c/N_{s0} and $N_c/N_{s\infty}$ are most important in controlling the shape of the stress–strain curves and the shape of the deformed body, with their absolute values fixed by the drawing forces. Displacement boundary conditions were imposed in the form of a restraint in the vertical (z) direction of a surface node in the shoulder region, to simulate the action of the split collet grip, and vertical displacement of the top horizontal boundary. The strains at the surface of the model are compared with those observed for a cylindrical specimen stretched at 0.35 mm s^{-1} to a total deformation of 55 mm (an overall extension ratio of 2.1 for the gauge length) in *Figure 7*; the corresponding nominal stress–extension curve is shown in *Figure 2*. Axial extension ratios are compared; given the axisymmetry and the incompressibility, these extension ratios define the shape uniquely. The chosen parameters give a realistic representation of the neck shape. The agreement at the high strains, where the natural draw ratio of the material is approached, suggests that the natural draw ratio of the model material matches that of the real material. Observations at the other higher testing speeds produced strain distributions which were indistinguishable from that shown here. This implies that the stress is separable as a product of functions of strain and of strain rate.

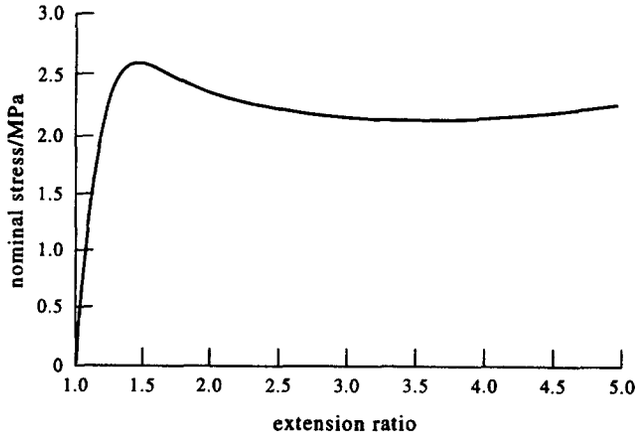

Figure 5 Typical nominal stress–strain curve for a necking polymer, with the maximum corresponding to the onset of necking and the minimum to the natural draw ratio

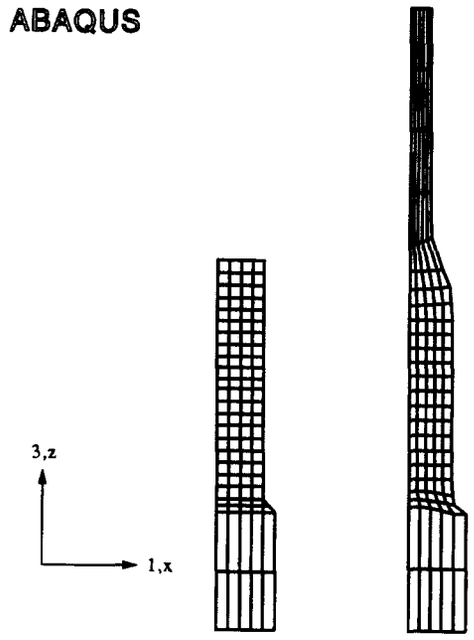

Figure 6 Axisymmetric finite element model of half of the cylindrical specimen, with the undeformed model on the left and the deformed model on the right

Table 1

Parameter set	N_c^* (MPa)	N_{s0}^* (MPa)	$N_{s\infty}^*$ (MPa)	η	β
A	0.33	6.64	2.13	0.2	2.0
B	0.26	11.22	6.15	0.6	1.5

Direct comparison of experimental and theoretical stress–strain curves has also proved possible. For the experimental data, observations at the neck centre were made for the large strain data. The theoretical curve is obtained from equation (6). For plane problems in the 1–3 plane, p can be eliminated using the condition $\sigma_{22} = 0$ to give

$$\sigma_{33} = N_c^*(\lambda_3^2 - \lambda_2^2) + N_s^*(I_1)(\lambda_3 b'(\lambda_3) - \lambda_2 b'(\lambda_2)) \tag{9}$$

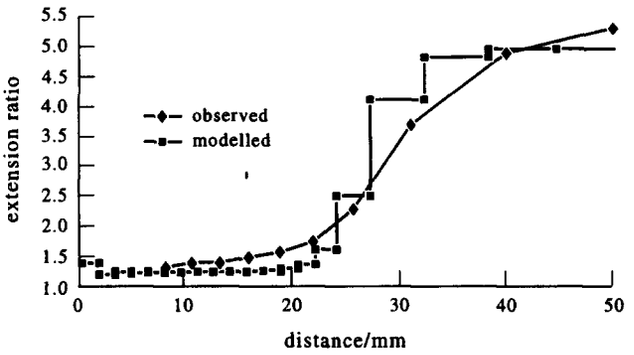

Figure 7 Comparison of measured and modelled surface strains for the cylindrical specimen

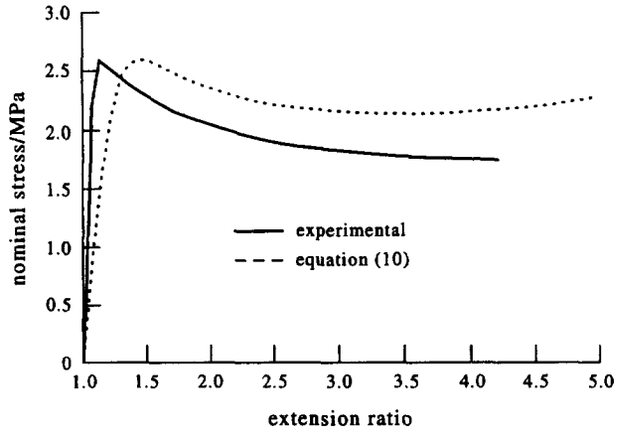

Figure 8 Experimental nominal stress–strain curve obtained from the cylindrical specimen by image analysis, compared with the theoretical curve corresponding to parameter set A of *Table 1*

For uniaxial stretching along the 3 axis, the incompressibility condition ensures that $\lambda_2 = \lambda_3^{-1/2}$ and the use of equation (8) gives the nominal stress:

$$\sigma_{33}^n = N_c^*(\lambda_3 - \lambda_3^{-2}) + N_s^*(I_1)(b'(\lambda_3) - \lambda_3^{-3/2}b'(\lambda_3^{-1/2})) \tag{10}$$

which is plotted in *Figure 8* using the values of parameter set A of *Table 1*. The peak in the nominal stress occurs at a higher extension ratio than that observed experimentally; this is a fundamental limitation of the theory. The experimental curve was obtained using the cylindrical specimen and stretching at a constant speed, corresponding to an initial shear rate of $0.01\ s^{-1}$.

Planar extension data

A comparison of planar extension and uniaxial data shows that uniaxial data are insufficient to define the parameters accurately. We demonstrate this using the parameter sets A and B as defined in *Table 1*. Set A was chosen on the basis described above of fitting the Ball *et al.* model[2] to uniaxial data, and was shown to produce realistic results for both uniaxial and planar extension behaviour. Set B gives non-physical behaviour, and is used to demonstrate that parameters which provide good fits to uniaxial data can also give totally unrealistic predictions for planar extension data. In *Figure 9* we plot the nominal stress as defined by equation (1) for uniaxial stretching, for parameter sets A and B. The two curves are very similar. It will now be shown that for planar extension the parameter sets A and B give very different

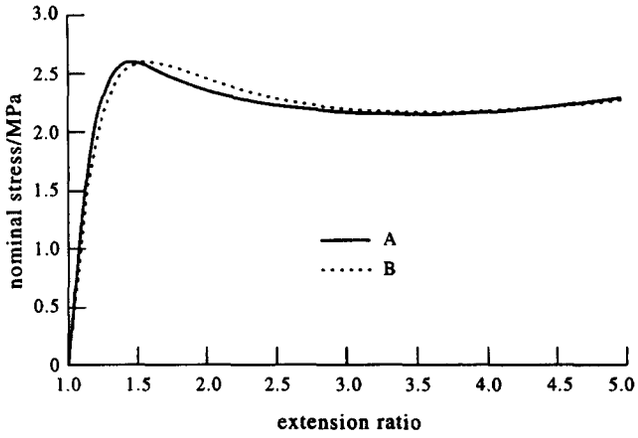

Figure 9 Comparison of uniaxial stress–strain curves corresponding to data sets A and B of *Table 1*

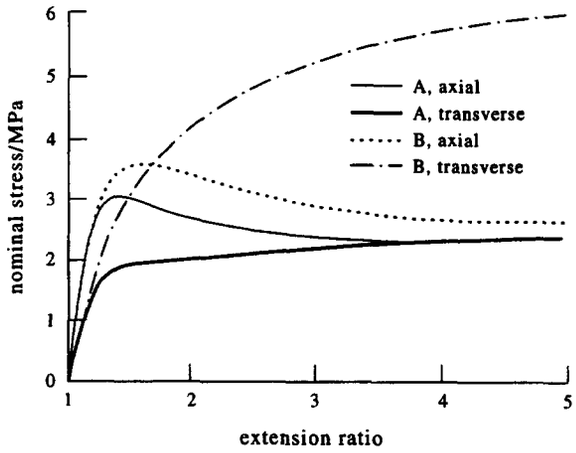

Figure 10 Comparison of stress–strain curves for planar extension corresponding to data sets A and B of *Table 1*

predictions. For stretching in the 1–3 plane along the 3 axis, while applying the lateral restraint $\lambda_1 = 1$, the through-thickness extension ratio λ_2 is given by the incompressibility conditions as $\lambda_2 = \lambda_3^{-1}$. Equations (8) and (9) give the nominal drawing stress as

$$\sigma_{33}^n = N_c^*(\lambda_3 - \lambda_3^{-3}) + N_s^*(I_1)(b'(\lambda_3) - \lambda_3^{-2}b'(\lambda_3^{-1})) \tag{11}$$

For this deformation, $\sigma_{11}^n = \sigma_{11}$ and using an equation analogous to (9) for the stress σ_{11}, the nominal lateral stress is given by

$$\sigma_{11}^n = N_c^*(1 - \lambda_3^{-2}) + N_s^*(I_1)(b'(1) - \lambda_3^{-1}b'(\lambda_3^{-1})) \tag{12}$$

Since $b'(1) = 1$, equation (12) implies that the stress approaches an asymptotic value of $N_c^* + N_{s\infty}^*$ at large stretches. The parameter η controls the rate of approach. In *Figure 10*, we plot the axial and transverse nominal stress as defined by equations (11) and (12) for both parameter sets A and B. The behaviours are grossly different, with the transverse stress exceeding the axial stress for set B. Thus, the parameter set B, while giving realistic uniaxial behaviour, is revealed as defining an unrealistic material.

This emphasizes the need to verify the material parameters using non-uniaxial experiments. We cannot perform a true planar extension test because our material does not deform homogeneously. However, the experiment in the previous section, in which specimens of the geometry illustrated in *Figure 3* are stretched using

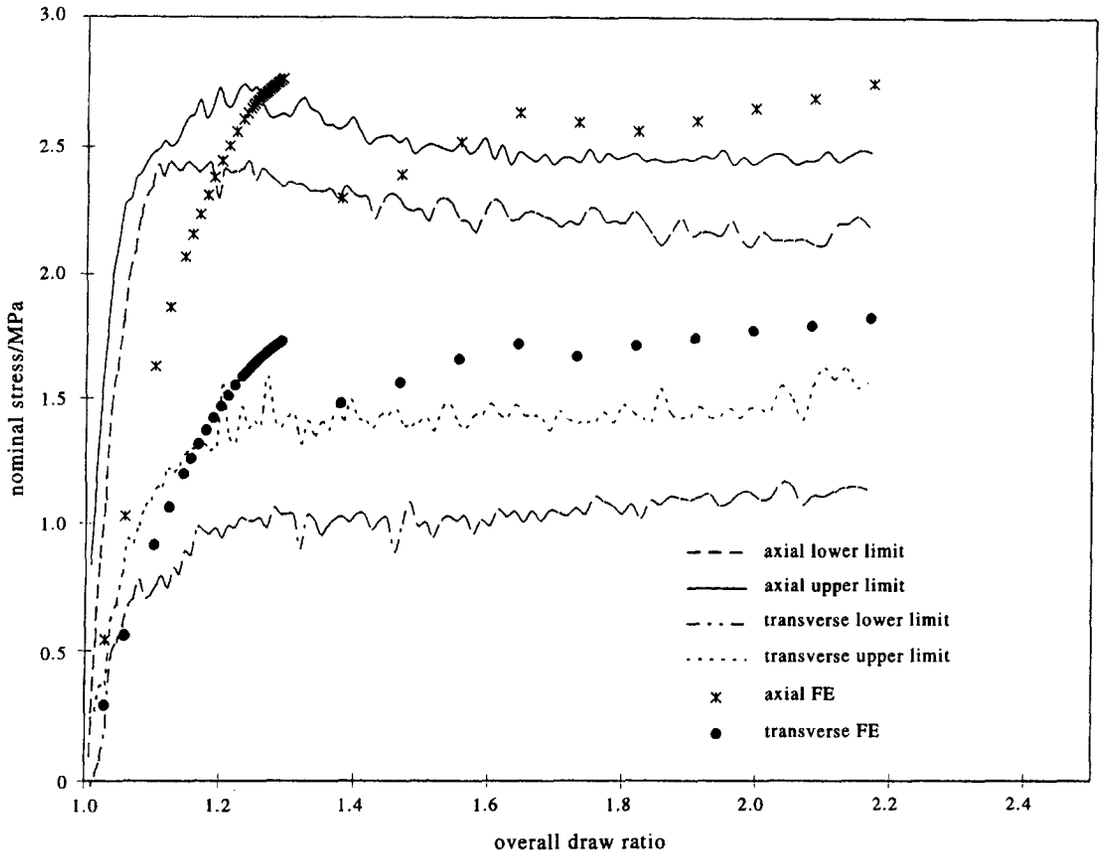

Figure 11 Forces arising from planar extension, for experiments on the specimen of *Figure 3*, and from the finite element model of *Figure 16*. The experimental results are an average of five experiments, with the upper and lower limits spanning a 90% confidence interval

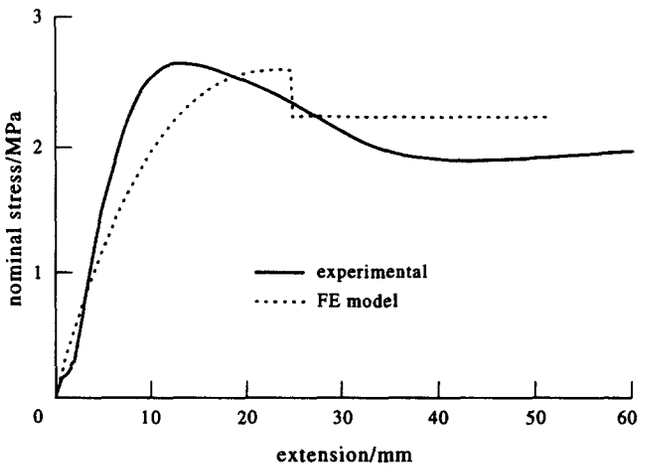

Figure 12 Nominal stress–extension curves for the cylindrical specimen at an initial strain rate of 0.01 s^{-1}, and for the corresponding finite element model

boundary conditions similar to planar extension, can provide the required data. In *Figure 11* we compare experimental and predicted stresses for such an experiment conducted at a shear rate of 0.01 s^{-1}. Both axial and lateral stresses are compared. The predictions are from a finite element model of the process, described in the next section, made using the material data defined by parameter set A of *Table 1*. The predictions conform realistically with the observed stresses. Larger values of η than the 0.2 value of set A tend to give lateral stress predictions which are too high, as would be expected from the behaviour of the theory in planar extension when parameter set B is used and η has the value 0.6. These findings support the value for η of 0.23 originally proposed by Ball *et al.*[2].

Effectiveness of model

This section explores the validity of the model as defined by equations (6) and (7) with parameter values given as set A in *Table 1*. As part of the process of assessing these material parameters, some degree of verification has already been achieved in the previous section. In this section we examine the predictions of shapes and drawing forces for both uniaxial geometries and for the planar extension test.

For the uniaxial tests on the specimens of circular cross-section of *Figure 1a*, the force predictions of the finite element model of *Figure 6* are compared with experiment in *Figure 12*. The experiment, the same as that associated with *Figure 8*, was carried out at 0.7 mm s^{-1} corresponding to an initial shear rate of 0.01 s^{-1}. The peak in the modelled force occurs at a higher extension than that observed, as would be expected from the similar behaviour in the stress–strain curve of *Figure 8*. The other clear discrepancy shown in *Figure 12* is the abruptness of the model load drop after the peak. We believe this to be a direct consequence of the elastic nature of the constitutive law. The load drop corresponds to a sudden extension of the elements in the neck and an accompanying high rate of strain in these elements. Because of the viscoelastic nature of the real material, such a high strain rate would be accompanied by a high stress, and this has the general effect of moderating the speed of neck formation and smoothing out changes in load. In contrast, the elastic solution can jump freely from one stable state to another.

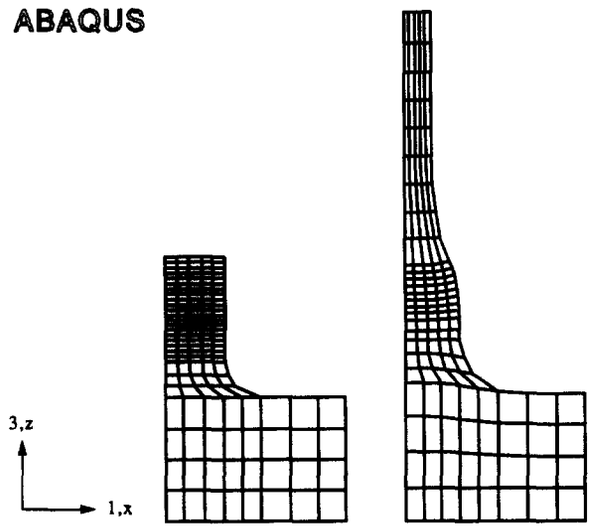

Figure 13 Finite element model of a quarter of the plane uniaxial specimen, with the undeformed model on the left and the deformed model on the right

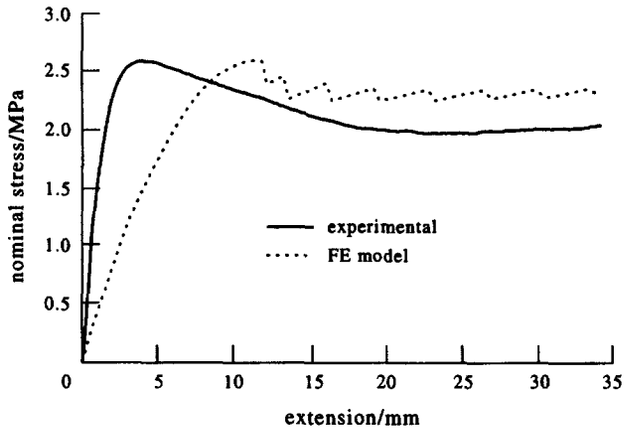

Figure 14 Nominal stress–extension curves for the plane uniaxial specimen at an initial strain rate of 0.01 s^{-1}, and for the corresponding finite element model

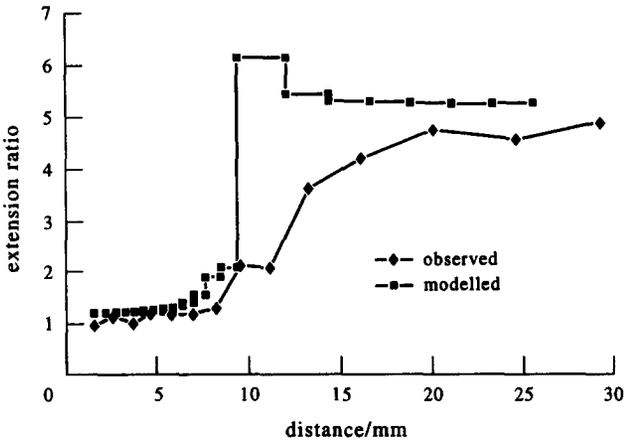

Figure 15 Comparison of measured and modelled surface strains for the plane uniaxial specimen

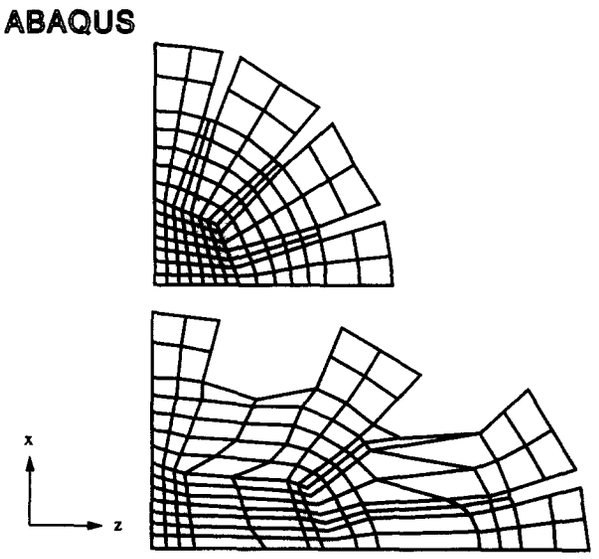

Figure 16 Finite element model of the planar extension experiment, with the undeformed model above and the deformed model below

The modelling of the shapes of the cylindrical specimens is well represented by *Figure 7*, which concerns the shape at a deformation of 55 mm, when the neck has fully formed. The quality of the modelling differs significantly from this only at the deformation corresponding to the abrupt fall in load mentioned above. Here, the transition from unnecked to necked material occurs over a much shorter distance in the model than in the specimen. This corresponds to the unrealistically high strain rate mentioned above.

Uniaxial experiments were also performed on sheet dumb-bell specimens of the type illustrated in *Figure 1b*. The two-dimensional model of the specimen, consisting of four-noded finite elements, is shown in *Figure 13* in its undeformed and deformed states. The associated nominal stress–extension curve is shown in *Figure 14*, using the parameter set A for the finite element analysis and carrying out the experiment at a constant testing speed corresponding to an initial shear strain rate of 0.01 s^{-1}. The oscillations in the predicted nominal stress are the result of the fall in load of each row of elements as it goes through the neck. For this model the extensions of elements in the same horizontal row are very similar to one another, so the load drop occurs at the same instant for the whole row, affecting the total load in the specimen. For the cylindrical specimen of *Figure 12*, the effect is masked as extension varies more between elements in the same row. The deformation field of the experiment, as obtained using image analysis, is compared with the finite element prediction in *Figure 15* in terms of axial draw ratio along the specimen axis. The change in the extension ratio is again more abrupt in the model than in the specimen, more markedly so than for the cylindrical specimen of *Figure 7*.

For the planar extension experiments, the finite element model is shown in the undeformed and deformed states in *Figure 16*. The axial and lateral drawing forces have been compared in *Figure 11*. In the model, necks develop between the separating grips and spread into the specimen in essentially the same manner as observed experimentally. A more quantitative comparison, of axial draw ratio, is made using contour plots in *Figure 17*. The experimental plot is derived from measurements on the mesh printed on the specimen (shown in *Figure 4*) and gives slightly less spatial resolution than is available in some regions of the finite element model. This means that small regions of high strain predicted by the model may not be observed experimentally because they have in

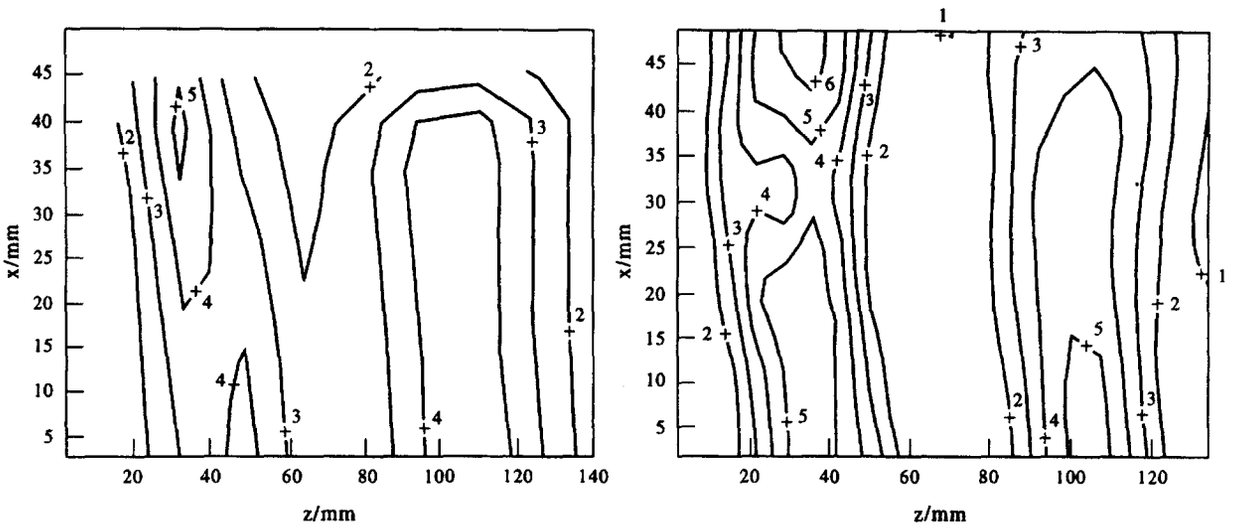

Figure 17 Contour plots of axial extension ratio λ_z for the experimental results (left) and the finite element model of *Figure 16* (right)

effect been averaged out. The overall agreement is good, with the only notable discrepancies being such high strain regions.

CONCLUSIONS

There has been other work on the quantitative modelling of necking polymers, but in contexts different from the present one of semi-crystalline polymers at high temperatures. Boyce *et al.*[6] and Wu and van der Geissen[7] have modelled the necking of glassy polymers at room temperature. In both these cases, the mechanism of necking is assumed to reside in rate-dependent plasticity. As argued previously[1], the rate dependence of polypropylene is too weak at 150°C to be associated with the mechanism of necking. However, the rate dependence strengthens as the test temperature is lowered, and so we would expect it to become strong enough to cause necking, or at least strain softening, at sufficiently low temperatures. This suggests that there are, in general, two strain softening processes in polypropylene. This is not unreasonable, given the observed double yield points at room temperature in polyethylene[8,9].

The modified Ball *et al.* model has been shown to provide an adequate representation of the three different deformation modes studied. The neglect of rate dependence leads in all cases to an unrealistically sudden drop in load after the formation of the neck. The other discrepancy—the prediction of the onset of necking at too high an extension—is also an inherent property of the model. Some preliminary studies have shown that the introduction of rate dependence into the present model (by making N_s a function of shear strain rate) has the effect of lessening the abruptness of the load drop after necking, and also of creating a smoother and more realistic neck shape. As it stands, the present elastic model can be viewed as a useful first-order theory, for which the introduction of rate dependence would provide further refinement and predictions of greater accuracy. Such a model is to be the subject of a future paper.

The principal practical advantage of the elastic model is that it requires fewer computing resources than alternative approaches. One such alternative is the elastic–plastic constitutive model. For a quantitative comparison, a tensile specimen has been modelled with a plane stress ABAQUS analysis of 370 four-noded elements, using both the present modified Ball *et al.* model and an elastic–piecewise linear plastic model as the constitutive law, with parameters such as to give approximately the same uniaxial stress–strain curves. Running on a Sun SPARC-20 workstation, the total computing times required to achieve the same overall deformation, corresponding to the onset of necking, were 124 s for the elastic–plastic model and 47 s for the elastic model. A complete description of the material would require a non-linear viscoelastic model, which can be expected to be more computationally intensive than the elastic–plastic approach.

ACKNOWLEDGEMENT

We wish to thank Mr P. Caton-Rose for generating the analyses used for the comparison of computing times for the elastic and elastic–plastic solutions.

REFERENCES

1. Sweeney, J. and Ward, I. M., *J. Mech. Phys. Solids*, 1996, **44**, 1033.
2. Ball, R. C., Doi, M., Edwards, S. F. and Warner, M., *Polymer*, 1981, **22**, 1010.
3. Sweeney, J. and Ward, I. M., *J. Rheol.*, 1995, **39**, 861.
4. Haynes, A. R. and Coates, P. D., *J. Mater. Sci.*, 1996, **31**, 1843.
5. Neale, K. W. and Tugcu, P., *J. Mech. Phys. Solids*, 1985, **33**, 323.
6. Boyce, M. C., Montagut, E. L. and Argon, A. S., *Polym. Eng. Sci.*, 1992, **32**, 1073.
7. Wu, P.-D. and van der Geissen, E., *Int. J. Plasticity*, 1995, **11**, 211.
8. Brooks, N. W. J., Duckett, R. A. and Ward, I. M., *Polymer*, 1992, **33**, 1872.
9. Brooks, N. W. J., Duckett, R. A. and Ward, I. M., *J. Rheol.*, 1995, **39**, 425.